

19. Horton, S., Meredith, A., Richardson, J. A. & Johnson, J. E. Correct coordination of neuronal differentiation events in ventral forebrain requires the bHLH factor MASH1. *Mol. Cell. Neurosci.* **14**, 355–369 (1999).
20. Hendry, S. H. & Carder, R. K. Neurochemical compartmentation of monkey and human visual cortex; similarities and variations in calbindin immunoreactivity across species. *Vis. Neurosci.* **10**, 1109–1120 (1993).
21. Jones, E. G. GABAergic neurons and their role in cortical plasticity in primates. *Cereb. Cortex* **3**, 361–372 (1993).
22. Sidman, R. L. & Rakic, P. Neuronal migration, with special reference to developing human brain: A review. *Brain Res.* **62**, 1–35 (1973).
23. Fode, C. et al. A role for neural determination genes in specifying the dorsoventral identity of telencephalic neurons. *Genes Dev.* **14**, 67–80 (2000).
24. Tarabykin, V., Stoykova, A., Usman, N. & Gruss, P. Cortical upper layer neurons derive from the subventricular zone as indicated by *Svet1* gene expression. *Development* **128**, 1983–1993 (2001).
25. Kakita, A. & Goldman, J. Patterns and dynamics of SVZ cell migration in the postnatal forebrain: monitoring living progenitors in slice preparations. *Neuron* **23**, 461–472 (1999).
26. Preuss, T. Taking the measure of diversity: comparative alternatives in the model-animal paradigm in cortical neuroscience. *Brain Behav. Evol.* **55**, 287–299 (2000).
27. Rakic, P. Specification of cerebral cortical areas. *Science* **241**, 170–176 (1988).
28. Gleeson, J. G. & Walsh, C. A. Neuronal migration disorders: From genetic diseases to developmental mechanisms. *Trends Neurosci.* **23**, 352–359 (2000).
29. Jones, E. G. Cortical development and thalamic pathology in schizophrenia. *Schizophr. Bull.* **23**, 483–501 (1997).
30. Lewis, D. A. GABAergic local circuit neurons and prefrontal cortical dysfunction in schizophrenia. *Brain Res. Rev.* **31**, 270–276 (2000).
31. Haydar, T. F., Bambrick, L. L., Kruger, B. K. & Rakic, P. Embryonic organotypic slice cultures for analysis of proliferation, cell death and migration in the cerebral wall. *Brain Res. Protocols* **4**, 425–437 (1999).
32. Letinic, K. & Rakic, P. Telencephalic origin of human thalamic GABAergic neurons. *Nature Neurosci.* **4**, 931–936 (2001).

Acknowledgements

We thank J. E. Johnson for providing Mash1 antibodies and J. L. R. Rubenstein and S. Anderson for providing *Dlx1/2* antibodies. We also thank F. Miller for providing Ta1-LacZ plasmid. We are grateful to all colleagues in the laboratory of P. R. for their advice and comments on the manuscript.

Competing interests statement

The authors declare that they have no competing financial interests.

Correspondence and requests for materials should be addressed to P.R. (e-mail: pasko.rakic@yale.edu).

Regulation of AMPA receptor lateral movements

Aren J. Borgdorff & Daniel Choquet

CNRS UMR 5091, Université de Bordeaux 2, Bordeaux 33077, France

An essential feature in the modulation of the efficacy of synaptic transmission is rapid changes in the number of AMPA (α -amino-3-hydroxy-5-methyl-4-isoxazole propionic acid) receptors at post-synaptic sites on neurons^{1–4}. Regulation of receptor endo- and exocytosis has been shown to be involved in this process^{5–14}. Whether regulated lateral diffusion of receptors in the plasma membrane also participates in receptor exchange to and from post-synaptic sites remains unknown. We analysed the lateral mobility of native AMPA receptors containing the glutamate receptor subunit GluR2 in rat cultured hippocampal neurons, using single-particle tracking and video microscopy. Here we show that AMPA receptors alternate within seconds between rapid diffusive and stationary behaviour. During maturation of neurons, stationary periods increase in frequency and length, often in spatial correlation with synaptic sites. Raising intracellular calcium, a central element in synaptic plasticity, triggers rapid receptor immobilization and local accumulation on the neuronal surface. We suggest that calcium influx prevents AMPA receptors from diffusing, and that lateral receptor diffusion to

and from synaptic sites acts in the rapid and controlled regulation of receptor numbers at synapses.

We measured the lateral mobility of native GluR2-containing AMPA receptors in the plasma membrane of rat cultured hippocampal neurons using 0.5- μ m latex beads coated with an antibody against the extracellular domain of GluR2. Each bead was held in contact with the surface of a neurite with laser tweezers for 5–10 s to allow binding to GluR2. After being released from the tweezers, the bead trajectory was followed by video microscopy for 200 s at 25 Hz with a spatial resolution of 5–10 nm, thus reflecting GluR2 movement (Fig. 1a and Supplementary Information).

At all developmental stages studied, AMPA receptors alternated between periods of rapid diffusive movement (blue in Fig. 1a) and periods of slow diffusion confined within a sub-micrometre area (red). Switching between the two types of movement occurred abruptly (within one video frame, or 40 ms). We divided receptor trajectories into episodes expressing one of these behaviours using a confinement index^{15,16} as discriminator (Fig. 1b). Periods with a low confinement index relate to free diffusive movement, whereas a high confinement index reflects slow and spatially restricted movement.

During neuronal maturation, the mean diffusion coefficient of AMPA receptor movement significantly decreased, the main drop occurring at 4–6 days *in vitro* (DIV) (Fig. 1c). The percentage of time spent in the confined state strongly increased as neurons matured. This was due to a 5-fold increase in the mean duration of the confined state and a 1.5-fold decrease in the mean duration of

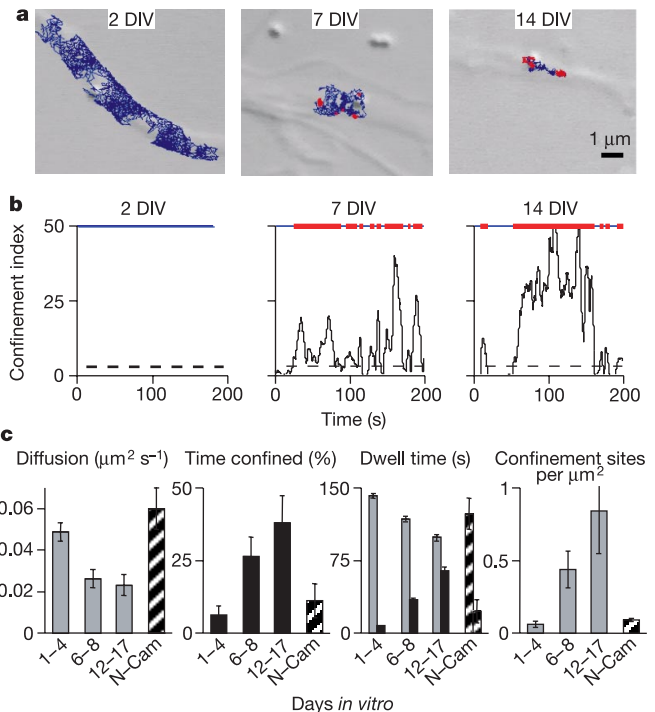


Figure 1 Lateral mobility of GluR2 decreases during neuronal maturation. **a**, Trajectories of GluR2-bound beads recorded for 200 s on the neurites of hippocampal neurons cultured for the indicated number of days (DIV), overlaid on the sample image. Confined and diffusive movement are shown respectively in red and blue. Scale bar, 1 μ m. **b**, Confinement index versus time for the trajectories in **a**. The dashed line shows the threshold for confined and diffusive episodes, as indicated above the plots (colour as in **a**). **c**, Histograms of mobility parameters for GluR2 (plain bars) and N-Cam (hatched bars). The diffusion coefficient, percentage of time spent in confined state, dwell time for diffusive (grey bars) and confined (black bars) episodes, and number of confinement zones divided by the spatial envelope (μm^2) of the trajectory are shown. 1–4 DIV, $n = 31$; 6–8 DIV, $n = 30$; 12–17 DIV, $n = 21$. N-Cam: 8–10 DIV, $n = 15$.

the diffusive state. This relates to the increased number of confinement sites per area of neurite explored by the receptors. By contrast, the mean diffusion coefficient during diffusive and confined periods only slightly decreased during maturation. For diffusive periods, values were (in $\mu\text{m}^2\text{s}^{-1}$, $\times 10^{-2}$): 1–4 DIV, 12 ± 0.9 ; 6–8 DIV, 8 ± 0.8 ; and 12–17 DIV; 6 ± 1 (mean \pm s.e.m.; $n = 31, 30, 21$, respectively). These values were about 30-fold higher than the diffusion coefficient during confined periods, with values of respectively 0.4 ± 0.08 , 0.2 ± 0.05 and 0.2 ± 0.03 (in $\mu\text{m}^2\text{s}^{-1}$, $\times 10^{-2}$). Together, these data show that reversible immobilization periods of AMPA receptors increase in length and frequency during neuronal maturation, in parallel with synaptogenesis¹⁷. For comparison, we recorded the mobility of N-Cam, an unrelated membrane-linked protein that does not accumulate at post-synaptic sites¹⁸ and usually displays diffusive movements on cell surface¹⁹. In 8–10-day-old cultures, when synapses are already numerous, N-Cam-bound beads diffuse most of the time (Fig. 1c). Thus, periods of GluR2 immobilization are not due to nonspecific hindrance of bead movement.

We found that zones where confinement of GluR2 occurs are

topographically related to synaptic structures. We located synapses with the pre-synaptic fluorescent marker FM1-43 and simultaneously mapped AMPA receptor movement with a bead (Fig. 2a). Receptors express confined movements more often on neurites that display a high level of FM1-43 staining (Fig. 2b) ($n = 35$, $P < 0.0005$, Spearman's paired test that the proportion of FM1-43 staining and fraction of time anchored are related). For quantification, we measured the distance between sites of confinement and the border of the nearest FM1-43 stain (FM–stop distance) as well as distances between adjacent FM1-43 stains for the concerned neurite (FM–FM distance). The distribution of FM–stop distances was strongly skewed towards shorter distances when compared with the distribution of FM–FM distances (Fig. 2c). On neurites that displayed FM1-43 staining, 51% of the confinement sites ($n = 35$ sites on 24 cells) were less than $0.5\mu\text{m}$ from an FM1-43 stain. Notably, receptors were often seen to halt only briefly in these regions (mean dwell time 24 ± 9 s, $n = 11$) and to switch from one FM region to the other (Fig. 2a). These results show that around synapses there is a region of low receptor diffusion. This may

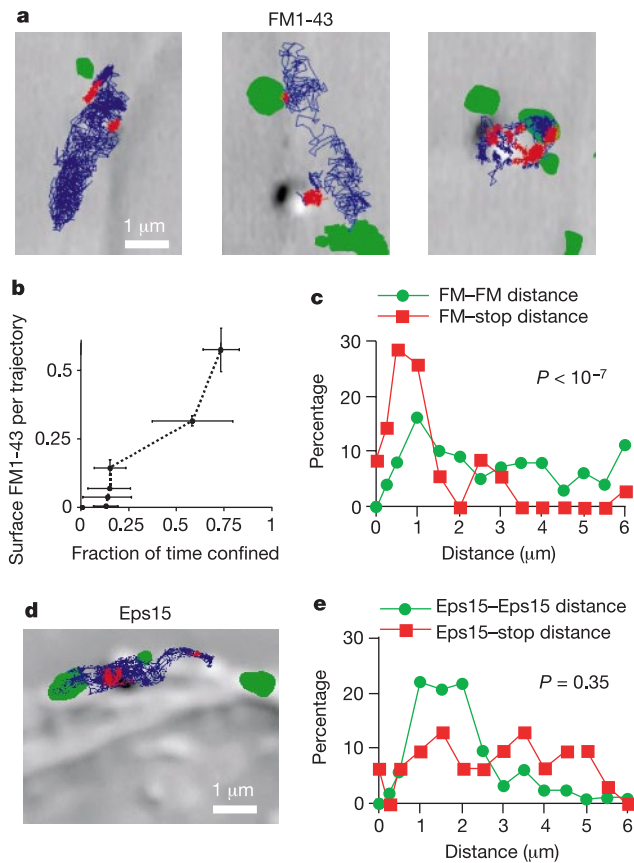


Figure 2 GluR2 stops reversibly at synaptic sites. **a**, Examples of the relation between GluR2 movement and FM1-43 staining (green). Diffusive movement is in blue, confined movement is in red. **b**, Plot of the fraction of surface stained by FM1-43 in the trajectory surface over the fraction of time the trajectory is confined (five recordings per data point). **c**, Normalized distribution of the distances between confinement zones and nearest FM1-43 stain (red squares, 35 observations) and of the distances between nearest-neighbour FM1-43 stains (green circles, 100 observations). Distributions are statistically distinct ($P < 10^{-7}$, Student's *t*-test). **d**, GluR2 movement (colour as in **a**) on a neuron transfected with Eps15-GFP (green). Eps15-GFP stains mark endocytic pits. **e**, Quantification of the distances between confinement zones and nearest Eps15-GFP stain (red squares, 21 observations) and between nearest-neighbour Eps15-GFP stains (green circles, 280 observations).

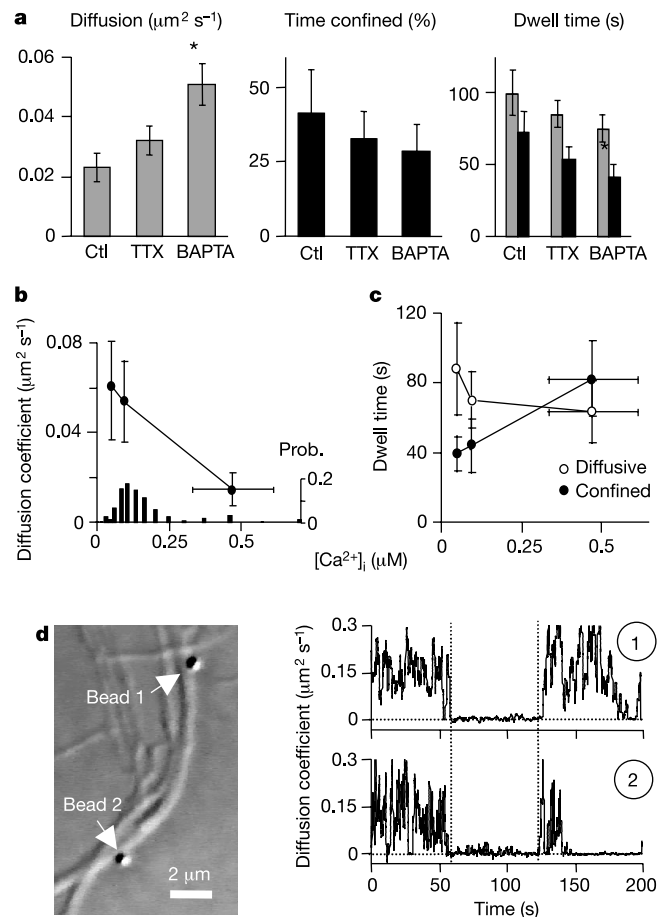


Figure 3 Spontaneous neuronal activity modulates GluR2 mobility. **a**, GluR2 mobility parameters in control conditions (Ctl, 12–17 DIV, $n = 21$), in the presence of $1\mu\text{M}$ TTX (12–15 DIV, $n = 61$), or $1\mu\text{M}$ TTX and intracellular BAPTA (12–13 DIV, $n = 23$). The diffusion coefficient, percentage of time spent in confined state, and dwell time for diffusive (grey bars) and confined (black bars) episodes are shown ($P < 5 \times 10^{-3}$, Student's *t*-test). **b**, Plot of GluR2 diffusion coefficient versus $[\text{Ca}^{2+}]_i$. (14–16 values per data point, 8–12 DIV). Black bars represent the $[\text{Ca}^{2+}]_i$ probability distribution (right axis) for 150 randomly sampled neurites. **c**, Diffusive and confined dwell times versus $[\text{Ca}^{2+}]_i$ for the data in **b**. **d**, Simultaneous recording of two GluR2-bound beads on a single neurite. Left, differential interference contrast image of the neurite (14 DIV). Right, diffusion coefficient versus time for each bead. Dotted lines indicate occasions where both beads stop and resume movement at about the same time.

correspond to reversible AMPA receptor binding to the external border of the post-synaptic density²⁰, in the way we observed for the reversible binding of glycine and mGluR5 (metabotropic glutamate) receptors to extra-synaptic clusters of gephyrin¹⁶ and Homer²¹, respectively.

Confinement zones not associated with FM1-43 staining could correspond to interaction of GluR2 with unstained synapses or with extrasynaptic structures such as receptor clusters^{16,21,22} or sites of endocytosis¹⁰. We tested the latter hypothesis by mapping endocytic pits with EGF-receptor pathway substrate 15 (Eps15) fused to green fluorescent protein (GFP)²³ while measuring GluR2 movement

(Fig. 2d). We found no correlation between Eps15 staining and zones of GluR2 confinement for 18 of 20 beads (Fig. 2e). However, on two occasions receptor immobilization occurred right on top of a pit (not shown). Thus, at best a small fraction of the confined episodes corresponds to arrest in endocytic pits.

Basal neuronal activity in synaptically connected neurons could also control AMPA receptor movement. Tetrodotoxin (TTX), which blocks sodium-dependent action potentials, slightly increased the mean diffusion coefficient and decreased the percentage of time spent in the confined state (Fig. 3a). Buffering intracellular calcium with BAPTA in the presence of TTX further increased diffusion and decreased confinement, mainly by significantly decreasing the mean duration of the confined state. That free intracellular calcium concentration ($[Ca^{2+}]_i$) is involved in the modulation of AMPA receptor mobility was further supported by the finding that receptors move more slowly in neurites having a spontaneously elevated $[Ca^{2+}]_i$ (Fig. 3b, 8–12 DIV). This was mainly due to an increase in the time spent in the confined state at increased $[Ca^{2+}]_i$ (Fig. 3c) ($P < 0.05$, Spearman's test). $[Ca^{2+}]_i$ in neurites distributed mainly (136 of 150 observations) between 0.05 and 0.25 μM (Fig. 3b, black bars). Together, these data indicate that, under resting $[Ca^{2+}]_i$ conditions, AMPA receptor mobility is relatively high, and that $[Ca^{2+}]_i$ has to be significantly raised to slow down receptor movement, as may occur during neuronal activity²⁴. We reasoned that if neuronal activity would modify GluR2 movement through brief elevations of $[Ca^{2+}]_i$, it would do so over the whole neurite in a temporally correlated manner. We recorded simultaneously the movement of two beads several micrometres apart on the same neurite. On a few occasions, we observed temporally correlated transitions from mobile to immobile and to mobile again (Fig. 3d) (on 18 couples of recorded beads, 10 of 110 such transitions occurred within 2 s of each other, whereas only about 2 should have been observed by chance only). These correlated transitions may reflect a spontaneous wave of physiological change in the neurite that freezes all receptors temporarily. Our data suggest that basal neuronal activity and/or $[Ca^{2+}]_i$ regulate, but do not fully determine, movement of AMPA receptors.

Activity-dependent elevation in post-synaptic $[Ca^{2+}]_i$ is known to be a central element in the regulation of synaptic transmission efficacy²⁴. Thus, it participates in both long-term depression (LTD) and potentiation (LTP) of synapses²⁵ as well as in fast exchange of AMPA receptors at synaptic sites²⁶. We investigated the effect of a localized $[Ca^{2+}]_i$ increase on receptor movement. This was achieved by photorelease of a caged Ca^{2+} ionophore with an ultraviolet (UV) laser focused on a small region near the receptor-coupled bead. In 76% of the trials ($n = 47$), activation of the Ca^{2+} ionophore produced a marked and rapid decrease in receptor mobility (Fig. 4a, b, and Supplementary Information). For these trials, the diffusion coefficient decreased on average to 20% (s.d. = 25%, range 0.2–80%) of the pre-stimulus value. The remaining population showed either no significant change in the diffusion coefficient (14% of the trials) or an increase (10% of the trials), as in control experiments ($n = 22$) with no Ca^{2+} ionophore added (Fig. 4b). The decrease in receptor mobility that followed photorelease could be partially prevented if neurons were pre-loaded with the Ca^{2+} chelator BAPTA ($n = 11$) (Fig. 4c), indicating the direct involvement of Ca^{2+} ions. In most cells, the effect lasted throughout the experiment (200 s). A partial recovery was observed in five of the trials. In comparison, the $[Ca^{2+}]_i$ increase induced by the photorelease lasted only a few seconds. The Ca^{2+} -induced receptor immobilization did not depend on the presence of functional synapses, because it was similar before and after synaptogenesis had started in our cultures (Fig. 4c). The Ca^{2+} -induced immobilization was not observed for N-Cam or mGluR5, another glutamate receptor whose basal mobility resembles that of GluR2 (ref. 21).

Activation of mGluR5 with its natural ligand glutamate leads to increased $[Ca^{2+}]_i$ and increased mGluR5 mobility²¹. In contrast,

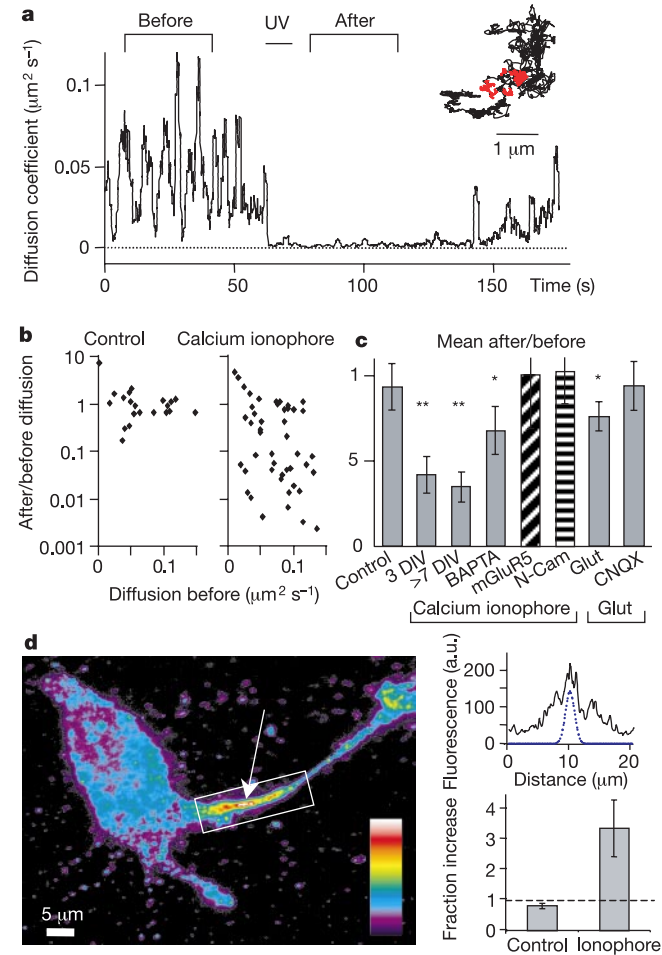


Figure 4 Local rises in intracellular calcium decrease GluR2 mobility and accumulate GluR2. **a**, Diffusion coefficient of GluR2 versus time during the uncaging of a caged calcium ionophore with a train of UV pulses (bar). Inset: GluR2 trajectory before (black) and after (red) uncaging. **b**, Ratios of the diffusion coefficient after and before uncaging versus the latter. (Before and after analysis windows are marked in **a**.) Each dot represents an experiment without (control, vehicle only) or with caged calcium ionophore (2–21 DIV). **c**, Mean values of the ratios of the diffusion coefficient after and before uncaging of caged calcium ionophore or caged glutamate (Glut), as indicated. From left to right: GluR2 with vehicle only (control), GluR2 with caged ionophore at 3 DIV ($n = 21$), at >7 DIV ($n = 26$), pre-loaded with BAPTA, mGluR5 and N-Cam with caged ionophore, GluR2 with caged glutamate without or with CNQX. Double asterisk, $P < 10^{-4}$; asterisk, $P < 0.05$; Student's paired t -test. **d**, Left, pseudo-colour image of the immunostaining of surface GluR2 on a neuron challenged for 5 min with repeated uncaging (arrow) of the caged calcium ionophore. Right, top, linescan intensity profile along the white box indicated in left panel. Dashed line indicates UV radiation intensity profile. a.u., arbitrary units. Right, bottom, mean percentage of increase in fluorescence intensity in the flashed region when compared with an adjacent unflashed region of the same neurite for control experiments (vehicle only, $n = 7$) and with the caged ionophore ($n = 9$) ($P < 0.015$, Student's t -test).

release of caged glutamate in the proximity of GluR2-bound beads induced an average decrease in GluR2 diffusion down to 33% (s.d. = 28%, range 0.3–76%) of the pre-stimulus value in 48% of the trials ($n = 35$) (Fig. 4c). In total, the effect of glutamate was significant, but less robust than that of the caged Ca^{2+} ionophore. The slowdown of receptor movement by glutamate could be prevented by a mixed AMPA/NMDA antagonist (50 μM 6-cyano-7-nitroquinoxaline-2,3-dione, CNQX; $n = 16$) (Fig. 4c), but not by an NMDA-specific antagonist (100 μM D(-)-2-amino-5-phosphonovaleric acid, AP5; $n = 12$) (data not shown).

Finally, we found that a series of repetitive localized $[\text{Ca}^{2+}]_i$ increases triggered by photorelease of the caged ionophore induced within minutes a major local accumulation of GluR2 on the neuronal surface (Fig. 4d). The same protocol did not trigger local accumulation of the coated pit protein Eps15 (not shown), nor was GluR2 accumulation observed when applying UV flashes in the absence of the caged ionophore. The most straightforward explanation for the calcium-induced increase in GluR2 density is that receptors accumulate over time as a result of repetitive calcium-induced immobilization of receptors that pass the zone of uncaging by lateral diffusion. This receptor immobilization on the neuronal surface could arise from calcium-induced increase in the affinity of GluR2 for scaffolding elements²⁷ and/or recruitment of such elements.

GluR2-containing AMPA receptors move rapidly in the plasma membrane of cultured neurons and may cover large distances. They halt regularly and reversibly in confinement zones, mostly corresponding to reversible arrest near synaptic structures, but sometimes also originating from arrest in endocytic pits and from spontaneous neuronal activity. The exchange of AMPA receptors between the post-synaptic density and the extra-synaptic membrane through lateral diffusion could be a prerequisite to the receptors' endo- and exocytotic regulatory processes, which are linked to LTP^{1,2,11,28} and LTD^{3,6,7,9,14} and are likely to occur preferentially outside the synapse. That local Ca^{2+} influx can regulate lateral GluR2 movement and local receptor concentration opens new avenues for the rapid control of AMPA receptor numbers at post-synaptic sites. Regulating the rate at which AMPA receptors can leave or enter synapses could lead to activity-dependent regulation of synaptic transmission. □

Methods

Cell culture and microscopy

Hippocampal neurons from rat embryos at embryonic day 18 were cultured on glass coverslips²⁹. For experiments with mGluR5, cultures were transfected with the complementary DNA encoding Myc-tagged mGluR5 (ref. 21). Video microscopy, latex bead preparation and manipulation with an optical trap were as described^{16,21}. Latex beads (0.5 μm diameter, Polysciences) were coated with anti-GluR2 (Chemicon), anti-N-Cam (a gift of R.-M. Mège) or anti-Myc (Roche diagnostics) antibodies. Neurons were mounted between two coverslips in culture medium with beads and 20 mM HEPES buffer (pH 7.2), kept at 37 °C and visualized under red illumination and differential interference contrast through a 100 \times , 1.4 numerical aperture PlanApo objective (Olympus). From each coverslip, we recorded bead trajectories of 200 s each on 1–4 neurons over a period of ~20 min. Bead binding to neurites was virtually suppressed by diluting 100-fold the anti-GluR2 antibody concentration at the bead surface.

Pre-synaptic staining with FM1-43

Neurons (10–17 DIV) were depolarized for 1 min in culture medium supplemented with 40 mM KCl and 10 μM FM1-43 (fluorescent and caged compounds from Molecular Probes), then washed and kept in standard medium containing 1 μM TTX (Sigma). After recording a bead trajectory, FM1-43 staining was visualized in the same recording field by epifluorescence (excitation/emission = 460–480/500–540 nm wavelength) with a Pentamax camera (Princeton Instruments).

Endocytic pit staining with Eps15

Neurons (7–9 DIV) were transfected with the cDNA encoding GFP-tagged Eps15, which is targeted to clathrin-coated pits²³. Bead trajectories were recorded 24 h after transfection. Visualization and quantification procedures were the same as for FM1-43.

Measurements of intracellular free calcium

Neurons were loaded with the dye Fura-2 AM (5 μM) for 20 min at 37 °C. At the start of the experiment, a neurite was chosen and its $[\text{Ca}^{2+}]_i$ determined from standard calibrated

Fura-2 ratiometric imaging (DG4 filter changer, Sutter Instruments). Receptor movement was then recorded from the Fura-2-imaged region.

Flash photolysis

To achieve fast and local rises in intracellular calcium or glutamate levels, we used local photorelease of respectively 1-(4,5-dimethoxy-2-nitrophenyl)ethyl (DMNPE)-caged Ca^{2+} ionophore A-23187 (25 μM) or N-(CNB-caged) L-glutamic acid (25 mM), which were added to the extracellular medium. For photorelease, a pulsed nitrogen UV laser (VSL 337, LSI) was focused as a diffraction-limited spot in the image field. The photorelease protocol consisted of 30 UV flashes (~3- μJ pulses at 1 Hz) close to the tracked bead. For the caged ionophore, GluR2 immobilization was usually achieved with a single UV flash. Control $[\text{Ca}^{2+}]_i$ imaging experiments performed with Fluo-3 in the presence of the caged ionophore verified that a single UV flash produced a rapid, substantial (>0.5 μM) and transient (mean decay time constant 2.5 s) increase in dendritic $[\text{Ca}^{2+}]_i$. For quantification, in each recording we compared the mean diffusion coefficient during 30-s periods before and after UV illumination. For BAPTA loading, cells were incubated for 15 min with 5 μM BAPTA-AM (Molecular Probes). For GluR2 accumulation, during 5 min, one burst (50 Hz) of ten UV pulses was delivered every 30 s. Cells were fixed immediately afterwards with 4% paraformaldehyde-sucrose to avoid permeabilization, and processed for immunostaining with anti-GluR2 and secondary antibodies. Experiments were performed on neurons at 4–6 DIV that were transfected with the cDNA encoding a GFP-tagged GluR2, to help cell recognition.

Bead tracking and data analysis

Positions of GluR2-bound beads were tracked on digitized video images^{16,21}. Diffusion coefficients for whole or parts of trajectories were calculated by fitting the first three points of the mean squared displacement (MSD) curves versus time. Plots of diffusion coefficients versus time were derived from MSDs calculated on contiguous trajectory stretches of 50 points. Confined movement is a period during which receptor movement is contained within a region smaller than that expected from free brownian movement. To detect periods of confined receptor movement, we calculated a confinement index¹⁵ as previously described^{16,21}. Confined periods were detected as stretches of positions having an index greater than 3.16 for 2.7 s or more. This threshold reflects a 99.3% likelihood to pertain to a confined movement. Distances from confinement zone to the nearest border of an FM1-43 stain were calculated from FM1-43 staining images made binary and overlaid with the corresponding bead trajectory with Metamorph 4.0 software (Universal Imaging Corporation). Data are given as mean \pm s.e.m., unless noted.

Received 15 February; accepted 2 April 2002; doi:10.1038/nature00780.

- Hayashi, Y. *et al.* Driving AMPA receptors into synapses by LTP and CaMKII: requirement for GluR1 and PDZ domain interaction. *Science* **287**, 2262–2267 (2000).
- Shi, S. H. *et al.* Rapid spine delivery and redistribution of AMPA receptors after synaptic NMDA receptor activation. *Science* **284**, 1811–1816 (1999).
- Carroll, R. C., Lissin, D. V., von Zastrow, M., Nicoll, R. A. & Malenka, R. C. Rapid redistribution of glutamate receptors contributes to long-term depression in hippocampal cultures. *Nature Neurosci.* **2**, 454–460 (1999).
- Shi, S., Hayashi, Y., Esteban, J. A. & Malinow, R. Subunit-specific rules governing AMPA receptor trafficking to synapses in hippocampal pyramidal neurons. *Cell* **105**, 331–343 (2001).
- Carroll, R. C., Beattie, E. C., von Zastrow, M. & Malenka, R. C. Role of AMPA receptor endocytosis in synaptic plasticity. *Nature Rev. Neurosci.* **2**, 315–324 (2001).
- Luthi, A. *et al.* Hippocampal LTD expression involves a pool of AMPARs regulated by the NSF–GluR2 interaction. *Neuron* **24**, 389–399 (1999).
- Beattie, E. C. *et al.* Regulation of AMPA receptor endocytosis by a signalling mechanism shared with LTD. *Nature Neurosci.* **3**, 1291–1300 (2000).
- Lin, J. W. *et al.* Distinct molecular mechanisms and divergent endocytotic pathways of AMPA receptor internalization. *Nature Neurosci.* **3**, 1282–1290 (2000).
- Wang, Y. T. & Linden, D. J. Expression of cerebellar long-term depression requires postsynaptic clathrin-mediated endocytosis. *Neuron* **25**, 635–647 (2000).
- Man, Y. H. *et al.* Regulation of AMPA receptor-mediated synaptic transmission by clathrin-dependent receptor internalization. *Neuron* **25**, 649–662 (2000).
- Lu, W. *et al.* Activation of synaptic NMDA receptors induces membrane insertion of new AMPA receptors and LTP in cultured hippocampal neurons. *Neuron* **29**, 243–254 (2001).
- Sheng, M. & Lee, S. H. AMPA receptor trafficking and the control of synaptic transmission. *Cell* **105**, 825–828 (2001).
- Noel, J. *et al.* Surface expression of AMPA receptors in hippocampal neurons is regulated by an NSF-dependent mechanism. *Neuron* **23**, 365–376 (1999).
- Luscher, C. *et al.* Role of AMPA receptor cycling in synaptic transmission and plasticity. *Neuron* **24**, 649–658 (1999).
- Simson, R., Sheets, E. D. & Jacobson, K. Detection of temporary lateral confinement of membrane proteins using single-particle tracking analysis. *Biophys. J.* **69**, 989–993 (1995).
- Meier, J., Vannier, C., Sergé, A., Triller, A. & Choquet, D. Fast and reversible trapping of surface glycoproteins by gephyrin. *Nature Neurosci.* **4**, 253–260 (2001).
- Fletcher, T. L., De Camilli, P. & Banker, G. Synaptogenesis in hippocampal cultures: evidence indicating that axons and dendrites become competent to form synapses at different stages of neuronal development. *J. Neurosci.* **14**, 6695–6706 (1994).
- Kiss, J. Z. & Muller, D. Contribution of the neural cell adhesion molecule to neuronal and synaptic plasticity. *Rev. Neurosci.* **12**, 297–310 (2001).
- Simson, R. *et al.* Structural mosaicism on the submicron scale in the plasma membrane. *Biophys. J.* **74**, 297–308 (1998).
- Nusser, Z. AMPA and NMDA receptors: similarities and differences in their synaptic distribution. *Curr. Opin. Neurobiol.* **10**, 337–341 (2000).
- Sergé, A., Fourgeaud, L., Hémar, A. & Choquet, D. Receptor activation and homer differentially control the lateral mobility of mGluR5 in the neuronal membrane. *J. Neurosci.* (in the press).

22. Pickard, L., Noel, J., Henley, J. M., Collingridge, G. L. & Molnar, E. Developmental changes in synaptic AMPA and NMDA receptor distribution and AMPA receptor subunit composition in living hippocampal neurons. *J. Neurosci.* **20**, 7922–7931 (2000).
23. Benmerah, A., Poupon, V., Cerf-Bensussan, N. & Dautry-Varsat, A. Mapping of Eps15 domains involved in its targeting to clathrin-coated pits. *J. Biol. Chem.* **275**, 3288–3295 (2000).
24. Ghosh, A. & Greenberg, M. E. Calcium signalling in neurons: molecular mechanisms and cellular consequences. *Science* **268**, 239–247 (1995).
25. Yang, S. N., Tang, Y. G. & Zucker, R. S. Selective induction of LTP and LTD by postsynaptic $[Ca^{2+}]_i$ elevation. *J. Neurophysiol.* **81**, 781–787 (1999).
26. Liu, S. Q. & Cull-Candy, S. G. Synaptic activity at calcium-permeable AMPA receptors induces a switch in receptor subtype. *Nature* **405**, 454–458 (2000).
27. Lee, H. K., Barbarosie, M., Kameyama, K., Bear, M. F. & Huganir, R. L. Regulation of distinct AMPA receptor phosphorylation sites during bidirectional synaptic plasticity. *Nature* **405**, 955–959 (2000).
28. Malinow, R., Mainen, Z. F. & Hayashi, Y. LTP mechanisms: from silence to four-lane traffic. *Curr. Opin. Neurobiol.* **10**, 352–357 (2000).
29. Hémar, A., Olivo, J. C., Williamson, E., Saffrich, R. & Dotti, C. G. Dendroaxonal transcytosis of transferrin in cultured hippocampal and sympathetic neurons. *J. Neurosci.* **17**, 9026–9034 (1997).

Supplementary Information accompanies the paper on Nature's website (<http://www.nature.com/nature>).

Acknowledgements

This work was supported by grants from the Centre National de la Recherche Scientifique and the Conseil Régional d'Aquitaine. A.J.B. was supported by the Fondation pour la Recherche Médicale and an EC (European Commission) Marie Curie Training fellowship. We thank P. Osten for his gift of GluR2–GFP cDNA, A. Benmerah for the gift of the Esp15–GFP cDNA, and R.-M. Mège for the gift of anti-N-Cam. We thank P. Ascher for his support during early phases of this work; C. Mulle, A. Hémar and L. Cognet for their comments on the manuscript; and F. Rossignol for cultures of hippocampal neurons.

Competing interests statement

The authors declare that they have no competing financial interests.

Correspondence and requests for materials should be addressed to D.C. (e-mail: dchoquet@u-bordeaux2.fr).

Annexin II light chain regulates sensory neuron-specific sodium channel expression

Kenji Okuse*, Misbah Malik-Hall*, Mark D. Baker*, W-Y. Louisa Poon*, Haeyoung Kong†, Moses V. Chao† & John N. Wood*

* Department of Biology, University College London, Gower Street, London WC1E 6BT, UK

† Molecular Neurobiology Program, Skirball Institute for Biomolecular Medicine, Departments of Cell Biology and Physiology and Neuroscience, New York University School of Medicine, New York, New York 10016, USA

The tetrodotoxin-resistant sodium channel $Na_v1.8/SNS$ is expressed exclusively in sensory neurons and appears to have an important role in pain pathways^{1,2}. Unlike other sodium channels, $Na_v1.8$ is poorly expressed in cell lines even in the presence of accessory β -subunits³. Here we identify annexin II light chain^{4,5} (p11) as a regulatory factor that facilitates the expression of $Na_v1.8$. p11 binds directly to the amino terminus of $Na_v1.8$ and promotes the translocation of $Na_v1.8$ to the plasma membrane, producing functional channels. The endogenous $Na_v1.8$ current in sensory neurons is inhibited by antisense downregulation of p11 expression. Because direct association with p11 is required for functional expression of $Na_v1.8$, disrupting this interaction may be a useful new approach to down-regulating $Na_v1.8$ and effecting analgesia⁶.

Voltage-gated sodium channels initiate and propagate action potentials in excitable cells. Ten distinct pore-forming α -subunits of voltage-gated sodium channels have been identified⁷. Expression of the tetrodotoxin-resistant (TTX-resistant) sodium channel

$Na_v1.8$ (also known as SNS/PN3 or SCN10a) is restricted to small-diameter C-fibre-associated sensory neurons¹. Behavioural studies on $Na_v1.8$ null mutant mice have shown that $Na_v1.8$ helps in the detection of noxious thermal, mechanical and inflammatory stimuli².

The α -subunits of sodium channels are known to associate with auxiliary β -subunits that promote functional channel expression^{3,8}. Microinjection of $Na_v1.8$ complementary DNA into the nuclei of superior cervical ganglion (SCG) neurons results in the robust expression of a sodium current that shows exactly the same biophysical properties as those observed in dorsal root ganglia (DRG) neurons⁹. In contrast, Chinese hamster ovary (CHO), African green monkey kidney (COS-7), human embryonic kidney (HEK-293) and other mammalian cell lines express few or no detectable $Na_v1.8$ channels after introduction of $Na_v1.8$ cDNA⁹, and the expressed channel shows different properties from the endogenous DRG current in these cell types¹⁰ even in the presence of auxiliary β -subunits (M.D.B., unpublished observations). These observations suggest that $Na_v1.8$ requires a distinct specific subunit or permissive factor different from known β -subunits to promote $Na_v1.8$ functional expression on the plasma membrane.

Here we report the use of the yeast two-hybrid interactive screen to identify p11 (the annexin II light chain)^{4,5} as a previously unknown regulatory factor for $Na_v1.8$ functional expression. A rat sensory neuron cDNA library¹¹ was used to screen for proteins that interact with the N-terminal intracellular domain of rat $Na_v1.8$. Five identical positive clones coding for a full-length p11 were identified through their interaction with the N terminus of $Na_v1.8$. To test whether p11 binds to the N-terminal intracellular domain of $Na_v1.8$ *in vitro*, we expressed the green fluorescent protein (GFP)–p11 fusion protein in COS-7 cells, and expressed the N-terminal domain of $Na_v1.8$ as a glutathione S-transferase (GST) fusion protein, GST–SNS(I). GST–SNS(I) pulled down the GFP–p11 fusion proteins specifically and efficiently in an GST pull-down assay¹² (see Supplementary Information).

We examined the tissue distribution of the p11 transcript. North-

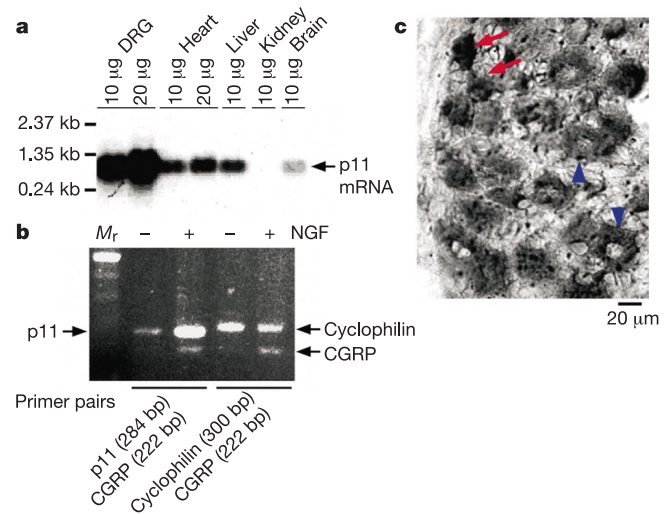


Figure 1 p11 mRNA is expressed in DRG neurons and is upregulated by NGF. **a**, Total RNA isolated from 2-week-old rat DRG, heart, liver, kidney and whole brain were subjected to Northern blot analysis. High levels of p11 mRNA are present in DRG and other tissues. **b**, RT-PCR analysis of p11 mRNA extracted from DRG neurons grown in the absence (-) or presence (+) of NGF for 7 days. A large increase of p11 mRNA is observed in response to NGF treatment. **c**, *In situ* hybridization shows that p11 mRNA is expressed in small- and large-diameter neurons in DRG. Damage-sensing small-diameter neurons (arrows in red) expressed p11 mRNA as well as large diameter neurons (arrowheads in blue). M_r , relative molecular mass.